INVESTIGATION OF THE MICROSCOPIC DAMAGE MECHANISM OF BAIJIU YEAST SPRAY DRYING
/
白酒酵母喷雾干燥微观损伤机制探究

Feng-Kui XIONG[1, 2)], Jing-Yu LI[1)], Yue-Jin YUAN[2*)], Ying-Ying XU[2)], Guang-Zhong HU[1)]
[1)] College of Mechanical Engineering, Library, Sichuan University of Science & Engineering, Yibin, Sichuan / China;
[2)] College of mechanical & Electrical Engineering, Shaanxi University of Science & Technology, Xian, Shaanxi / China
Corresponding author: Yue-jin Yuan. Tel: +86-029-86168810. E-mail: yyjyuan1@163.com
DOI: https://doi.org/10.35633/inmateh-72-32

Keywords: *Modified Sporidiobolus johnsonii A (MSJA); microscopic damage mechanism by spray drying; Combined drying; equipment design*

ABSTRACT
In this paper, the microscopic damage mechanism of Modified Sporidiobolus johnsonii A (MSJA) in spray drying was investigated. The results showed that at a water content of 0.21 or a temperature of 52 °C and at a water content of 0.07 or a temperature of 71°C, irreversible damage such as selective-permeable damage and collapse due to the transformation of the gel phase and the inverse-hexagonal phase of the phospholipid molecular layer of the cell membrane bilayer were the main reasons for the beginning of inactivation and large amount of inactivation of MSJA, respectively, in the spray-drying process.

摘要
本文对喷雾干燥中改性约氏掷孢 A(MSJA)的微观损伤机制进行了探究。结果表明：在含水率为 0.21 或温度达到 52 ℃时和含水率为 0.07 或温度达到 71 ℃时，细胞膜双层磷脂分子层的凝胶相和反六角相转变导致的选择透过性损伤和坍塌等非可逆性损伤分别是喷雾干燥过程中 MSJA 开始失活和大量失活的主要原因。

INTRODUCTION
As a culture throughout the Chinese civilization, baijiu is not only a treasure of the Chinese culture (*Liu Z. et al., 2023*), but also one of the pillars of the national economy, which has formed a trend of "blossoming" in the country *(Wang et al., 2021*). However, high-quality liquid active liquor yeasts (such as Modified *Sporidiobolus johnsonii A*, MSJA) are difficult to store and transport due to weak vitality, which seriously restricts the promotion and development of high-end baijiu in China (*Cheng, et al., 2022*). Current research generally agrees that drying the yeast to reduce its moisture content (*Cheng et al., 2021*), so that it is in a dormant state, is the optimal method to achieve its convenient transportation, long-term storage and promotion of the using (*Uki et al., 2021*). Meanwhile, spray drying has been occupying a dominant position in the field of drying microorganisms, such as yeast, by virtue of both high drying efficiency and low cost (*Gong P., et al. 2018*). Therefore, it is particularly important to investigate the microscopic damage mechanism of MSJA during the spray drying process to provide theoretical guidance for the subsequent design of the combined drying process with high efficiency and high survival rate of MSJA. (*Yuan et al., 2022*).

Regarding the investigation of damage mechanisms during spray drying of microorganisms: *Izu H. et al (2023)* investigated the hot air drying of sake cake containing Aspergillus niger and Saccharomyces cerevisiae and observed many free amino acids and a large amount of S-adenosylmethionine (SAM), which indicated that ribosomes of either *Aspergillus niger or Saccharomyces cerevisiae* were damaged during the hot air drying process. However, the critical temperature and mechanism of ribosome damage were not explored. *Yang H., et al (2023)* investigated the physical and thermal damage of Tetrahymena halophila during spray drying using flow cytometry, and obtained that heat-excited treatment prior to drying better maintains the integrity of the cell membrane, thus improving its survival rate in drying. However, the mechanism of cell membrane damage was not explored, and the critical temperature at which cell membrane integrity was damaged was not derived.

Therefore, the *MSJA*, which was jointly developed by the China Academy of Baijiu, was taken as the research object. Our team, carried out spray drying real-time sampling experiments, combined with Fourier Transform Infrared Scanning (FTIR), differential incubation, Scanning Electron Microscopy (SEM) and other microscopic detection means to explore the real damage mechanism of *MSJA* in the spray drying process.

MATERIALS AND METHODS

Experimental materials and experimental program design

The *MSJA* developed by the China Academy of Baijiu was used as the drying object in this experiment, and a small experimental spray dryer of Beicheng brand was used to carry out the spray drying experiment (*Al Zaitone, et al., 2022*). Spray dryer main drying tower height was h = 1.65 m, cylinder height h_1 = 1.14 m, diameter D = 800 mm, of which the effective drying section height was h_2 = 1 m, the bottom of the cone taper a = 60°, the bottom of the tower outlet aperture d = 150 mm. And set the material flow rate of 700 mL/h, hot air flow rate of 70 m³/h, and experimental variables inlet hot air temperature of 80, 100, 120℃ and 140℃, respectively. The experimental process and experimental equipment are shown in Fig. 1 (*Xiong, et al., 2022*).

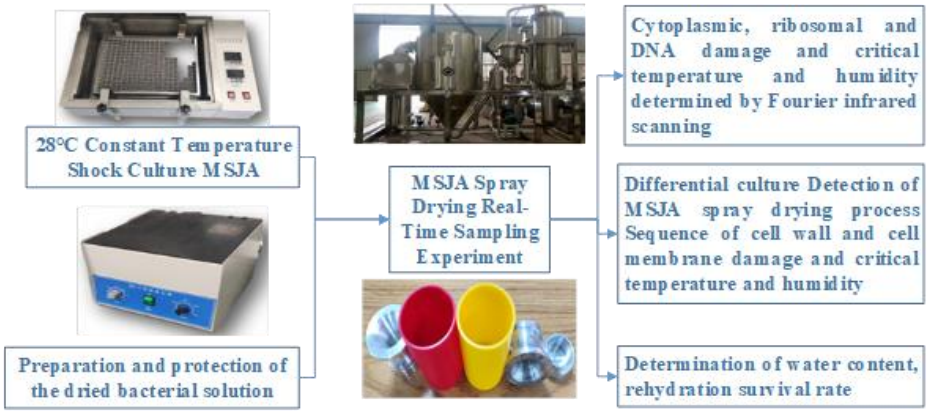

Fig. 1 - Experimental flow chart

Aiming at the difficulty of real-time sampling and nondestructive preservation of the spray drying process, this study developed a step-type double-cup body curved sampling cup with real-time efficient sampling and low-temperature nondestructive preservation system. In this system, firstly, the strong magnet at the bottom of the outer cup and the heat-insulating magnetic sticker on the outer surface work together to form a directional strong magnetic field at the mouth of the cup, which attracts the dry particles coated with carboxy iron powder (CIP) to enter into the inner cup, realizing high-efficiency sampling.

The first 20 cm of the curved inner cup is then formed by rotating a Bezier cubic curve (Eqs 1-3 below) with control points A, B, C, and D.

$$P(\mu)=\sum_{i=0}^{n} B_i^n(\mu)P_i \tag{1}$$

$$B_i^n(\mu)=\frac{n!}{i!(n-1)!}\mu^i(1-\mu)^{n-i} \tag{2}$$

$$P(\mu)=\mu^0(1-\mu)^3P_0+3\mu(1-\mu)^2P_1+3\mu^2(1-\mu)P_2+\mu^3(1-\mu)^0P_3=(1-\mu)^3P_0+3\mu(1-\mu)^2P_1+3\mu^2(1-\mu)P_2+\mu^3P_3 \tag{3}$$

This curved inner cup is used to optimize the hot air flow field at the cup mouth to achieve the goal of reducing hot air inflow into the sampling cup. The curved inner cup optimizes the hot air flow field at the mouth of the cup to achieve the goal of reducing the flow of hot air into the sampling cup under the premise of ensuring the stability of sampling. Together with the freezing layer filled with -40℃ antifreeze and the low-temperature and heat-insulating effect of the outer cup thermal insulation stickers, the samples can be stored at low temperatures (T≤4℃) without damage. Eventually, the step arrangement scheme and the cup mouth baffle were combined with the non-destructive installation of connecting magnets to achieve the goal of both real-time stable sampling and non-destructive cryopreservation of samples. The newly developed curved sampling cups and the pre-designed straight sampling cups are shown in Fig. 2.

A comparison of the bottom temperature (cryostat capability) and sampling quality (sampling stability) of the straight and curved sampling cups is shown in Fig. 3. The specific dimensions of the curved sampling cups were: the upper curved surface of the inner cup was 20 mm high with a minimum inner diameter of 18 mm; the lower part of the inner cup was 10 mm high with an inner diameter of 24 mm; the outer cup was 65 mm high with an outer diameter of 42 mm; and the wall thicknesses were all 2 mm. The dried particles were rehydrated in real-time by filling the cups with saline to constitute rehydrated sample sampling cups for microscopic observation of their drying damage.

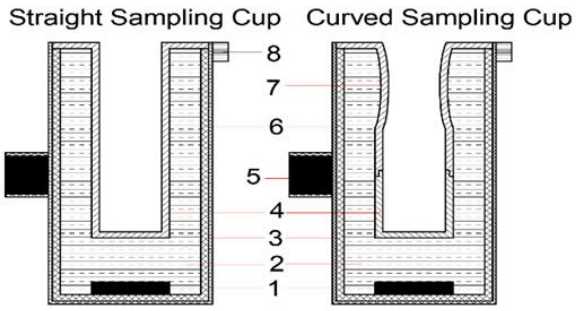

Fig. 2 - Schematic diagrams of curved and straight sampling cups with double cups

1-Connecting magnet; 2-Frozen layer; 3-Outer cup; 4-Lower part of inner cup; 5-Powerful magnets; 6-Heat and magnetic insulation tape; 7-Upper part of inner cup; 8-Wireless temperature and humidity sensors.

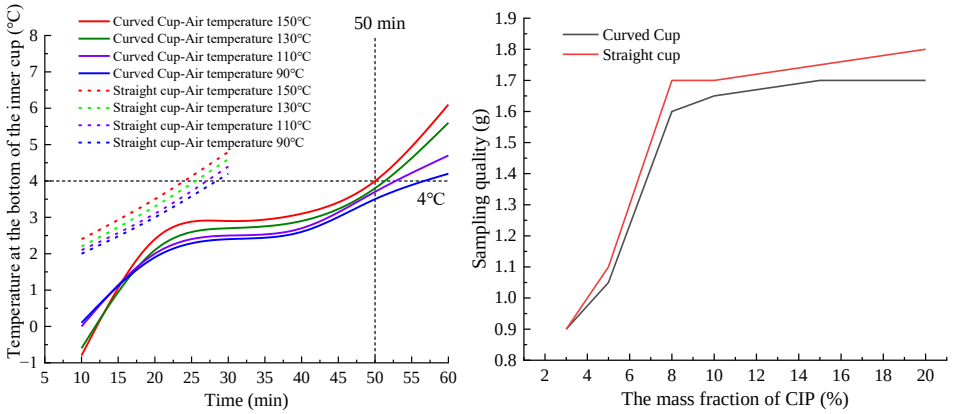

Fig. 3 - Comparison of bottom temperature and sampling quality of different types of sampling cups

The arrangement scheme is shown in Fig. 4, where the cups' rounded baffles together with the stepped arrangement scheme eliminate the sampling interference among the sampling cups (*Xiong et al., 2022*).

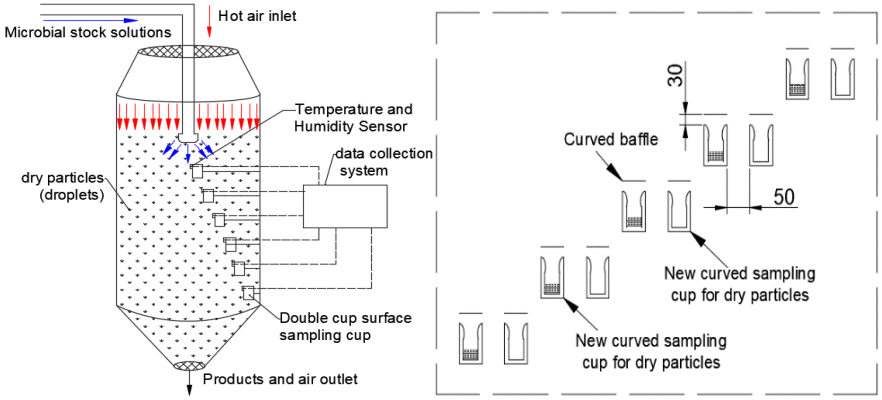

Fig. 4 - Schematic diagram of sampling experiment

Determination of experimental parameters

First, the temperature and humidity sensors arranged at the mouth of the sampling cups together with the data acquisition system collected and recorded the air temperature and humidity at each sampling point. Then, the samples in the sampling cups were removed and placed in a refrigerator at 4°C. Finally, the moisture content, rehydration survival rate, cell wall morphology, cell membrane, cell wall, protein and DNA damage and the order of damage were determined after the experiment was performed.

Determination of moisture content is as follows: preheat the moisture meter for 20 min→put the sample in the crucible→click the measurement button→read and record (*Spreutels et al., 2014*).

The rehydration survival rate of rehydrated samples was determined by the hypomethylated orchid staining + hemocyte counting method; and the formula for rehydration survival rate was (*Gomez-Narvaez F. et al., 2023*).

$$Q_v = \left\langle \frac{N_{us}}{N_T} \right\rangle \Big|_{three\text{-}fields} \times 100\% \quad (4)$$

Q_v - survival rate of rehydrated water; N_{us} - number of live bacteria (number of colourless organisms); N_T - total number of bacteria.

Determination of cell wall and cell mould damage

The MIC assay is a key step in the preparation (determining the amount of experiment reagents to be added) for the determination of *MSJA* cell membrane and cell wall damage. The steps of the assay are as follows: ① Prepare a sterile solution (20 groups in total) with deionized water according to Table 1, and filter it with a sterile membrane to remove bacteria, and at the same time, put YEPD medium into an autoclave at 120 ℃ for 15 min for spare, and finally prepare 24 triangular flasks numbered (labelled with the name of the additives and concentration) for spare. ② Add 10 ml of sterilized YEPD medium to each triangular flask according to the number, then add 10 ml of sterile solution prepared according to Table 1, and finally inoculate the dried *MSJA* particles in the triangular flasks at the ratio of 2% (v/v). ③ Firstly, the triangular flasks were placed in a constant temperature and humidity shaking incubator at 30°C and 70% humidity at 150 r/min for 12 h. Then, the absorbance of the culture solution in the well plates at 600 nm (OD600) was measured by UV spectrophotometer. Finally, the value of the minimum added concentration that significantly inhibits the growth of MSJA, obtained by graphing the data with Origin, is the MIC of the MSJA culture.

Table 1

Concentration for each component of the solution

Number	1	2	3	4	5	6
Penicillin (ug/ml)	0	0.156	0.312	0.624	1.248	2.496
Lysozyme (mg/ml)	0	0.156	0.312	0.624	1.248	2.496
Bovine bile salt (%)	0	0.032	0.064	0.128	0.256	0.512
NaCl (%)	0	0.25	0.5	1	2	4

In order to exclude the inhibitory effect of the four additives on the growth of healthy bacteria, and at the same time to use the sensitivity of *MSJA* bacteria to the four additives to determine the damage or collapse of the cell wall (membrane), the present study used the addition of 1/2 MIC concentration of the four additives to carry out the experiment. Specific experimental steps were as follows: ① YEDP medium containing the four additives was prepared according to 1/2 of the minimum inhibitory concentration obtained by MIC determination, and dried *MSJA* particles were inoculated into the newly made medium at the ratio of 2% (v/v) and incubated for 12 h. ② The number of viable bacteria and survival rate of *MSJA* were measured. ③ According to the change of *MSJA* sensitivity to penicillin, lysozyme, bovine bile salt and NaCl, the order of cell membrane and cell wall damage can be determined.

SEM observation of bacterial morphology and cell wall damage

Rehydrated samples were used: ① Bacteriophage was washed twice with PBS buffer, then fixed overnight with 4% (v/v) glutaraldehyde solution and washed again with PBS buffer. ② Sequentially dehydrated with alcohol at concentrations of 50%, 70%, 90% and 100% for 20 min. ③ Replaced ethanol by isoamyl acetate 2 times for 30 min each time (Note: before each washing or replacement of liquid, it was separated by centrifugation at 4000 rpm for 10 min, and the supernatant was discarded to take the precipitated bacterial bodies). ④ Put the bacteria obtained by centrifugation into a refrigerator at -40 ℃ for 8 h, and then remove the excess water and isoamyl acetate by freeze-drying. ⑤ The above-dehydrated samples were pasted onto specific copper plates with conductive double-sided tape. ⑥ The dehydrated samples were pasted onto specific copper plates with conductive double-sided tape. ⑦ The copper plates were sprayed with gold using an ion sputtering coater, and then the changes in the morphology of the bacteria were observed on the scanning electron microscope (SEM).

Dry pellet samples are used: ① Directly fix the dry pellet samples on the aluminium plate with conductive double-sided tape. ② Gold spraying treatment. ③ The damage of the *MSJA* cell wall can be obtained by observation under SEM.

Finally, the temperature and moisture content of each sampling point can be combined to obtain the critical temperature and moisture content of *MSJA* cell wall and cell membrane damage during spray drying, and then combined with SEM images can be analysed to obtain the kind of morphology that *MSJA* is less susceptible to be damaged during drying.

Determination of cytoplasmic, ribosome and DNA damage

Fourier transform infrared (FTIR) was used to determine the damage of *MSJA* cytoplasm, ribosomes and DNA (*Kandasamy, et al., 2022*). Firstly, the FTIR spectra of MSJA particles with different moisture contents during spray-drying were determined in the 3000-2700 cm^{-1} band associated with the C-H stretching of cell membrane lipids, the 1750-1500 cm^{-1} band associated with proteamides and the 1300-900 cm^{-1} band

associated with ribosomes (*Noghabi, et al., 2020*), respectively. Then, the second-order derivatives of the FTIR spectra were derived to obtain the corresponding FTIR second-order derivative maps. Finally, each FTIR second-order derivative profile was analysed in conjunction with microbiology to investigate the damage of cell membrane fatty acids, proteins and DNA in MSJA bacteria during spray drying.

The steps were as follows, ① Take the rehydrated sample and resuspend the bacteria in saline to make a resuspension solution. ② Take 0.03 mL of resuspended bacterial solution and evenly coat it on the zinc selenide window slice. ③ Put the window slice into a 40 ℃ hot air drying oven to dry for 1 h to remove the residual moisture, in order to avoid the interference of moisture on the spectrum during the experimenting process. ④ The infrared spectrometer was adjusted to the ATR reflectance mode, and the scanning was repeated 390 times at a resolution of 10 cm^{-1} in the range of 100~4000 cm^{-1} to obtain the Fourier infrared spectra of the samples. ⑤ The image data were processed with OMINIC 8.0 software, based on which the relevant absorption peaks were analysed and identified (the processing method was, firstly, 5-point smoothing of the spectral curves using the Savitzky-Golay equation, and then normalizing the spectrograms using the second-order derivatives).

RESULTS

Analysis of temperature, yeast moisture content and survival at sampling sites

Spray drying experiments of baijiu brewer's yeast were carried out according to the above experimental scheme, and then analysed graphically by Origin, and the resulting temperature of the mouth of each sampling cup, moisture content of dried particles and rehydration survival rate are shown in Fig. 5.

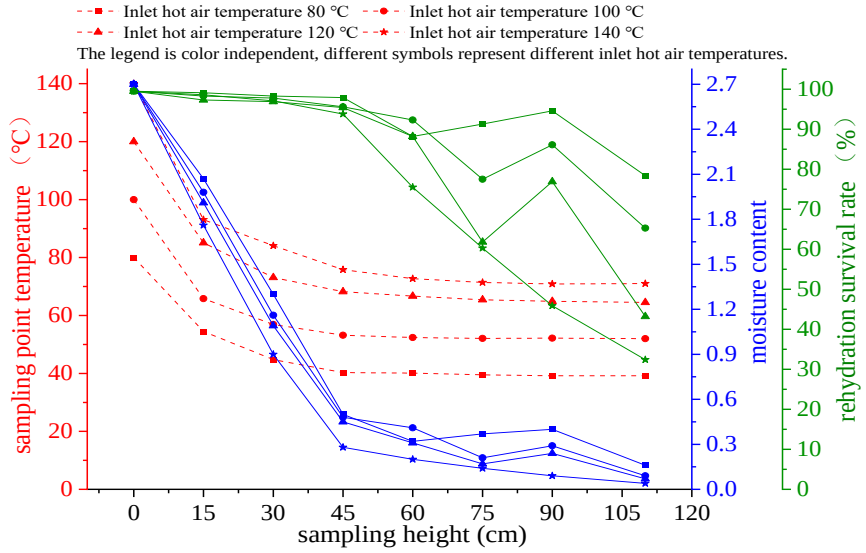

Fig. 5 - Temperature, moisture content and survival of yeast particles as a function of sampling altitude

From the temperature change curve in Fig. 5, it can be seen that the temperature in the drying tower generally decreases from top to bottom, but the rate of decrease decreases rapidly at the sampling heights of 15 cm and 45 cm, and stabilizes at 45 cm near the outlet temperature.

Combined with the moisture content curve and rehydration survival rate curve, it is easy to find that before the sampling height of 45 cm, the moisture content and temperature of the dried particles decreased sharply while the rehydration survival rate of the yeast in the particles almost did not decrease. This may be due to the fact that in the initial stage of downflow spray drying, the free water in the particles evaporates quickly and absorbs a large amount of heat from the hot air, and at the same time, it can also make the surface of the particles reach the equilibrium of the two gas-liquid species, which ensures that the yeast is in the "wet bulb temperature" environment and is almost not subject to thermal damage. The initial stage of microbial spray drying was called the "constant speed drying stage" (*Samborska et al., 2021*). After the sampling height of 45 cm, the free water in the pellet evaporates and the gas-liquid equilibrium on the surface of the pellet cannot be ensured, and the bacteria are exposed to the air temperature; at the same time, the bound water starts to evaporate, which leads to a gradual slowing down of the decrease of the moisture content of the pellet (reduced-rate drying stage) and a rapid decrease in the rehydration survival rate of *MSJA*. With the decelerated loss of bound water and the exposure of the bacteria to higher exit air temperatures, the *MSJA* bacteria were rapidly inactivated by both dehydration damage and thermal damage (*Hanae et al., 2018*).

Combined with the analysis of the moisture content and rehydration survival rate curves of spray-dried particles in Fig. 5, it is not difficult to conclude that the yeast particles are not completely top-down movement. Rather, the undried yeast particles will rise along the wall of the drying tower under the sheer force of the rising airflow along the wall to extend the drying time, and the specific trajectory is shown in Fig. 6 below.

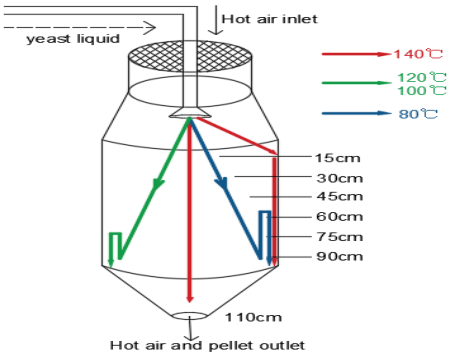

Fig. 6 - Trajectory of MSJA particles at each t air temperature

It is not difficult to find that the moisture content of the particles corresponding to the beginning of rapid inactivation of *MSJA* is between 0.2-0.32.

The order of cell wall (membrane) damage and temperature and moisture content determination

The effects of the four additives on *MSJA* growth at different concentrations as measured by the MIC experiment are shown in Fig. 7

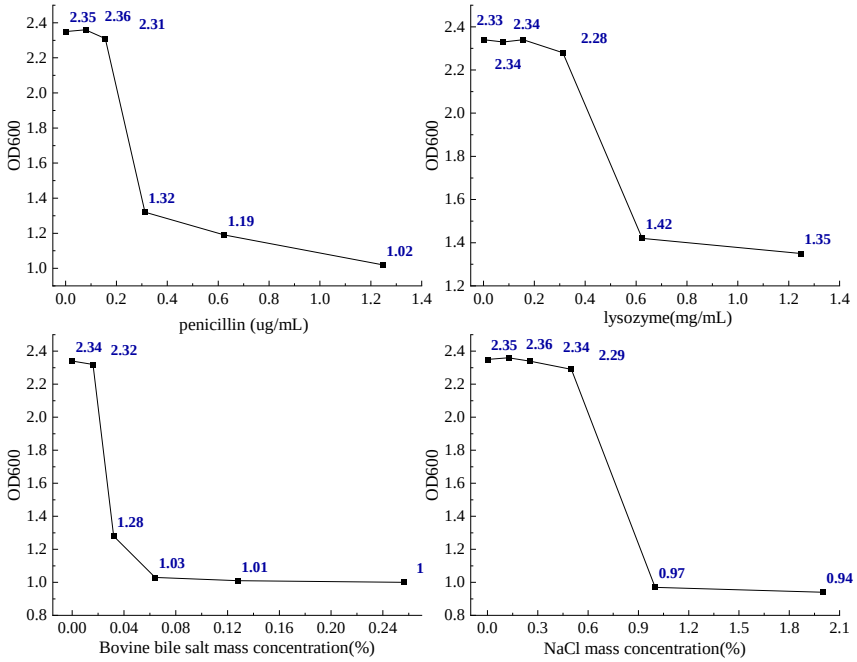

Fig. 7 - Effect of each concentration on yeast growth

From the analysis of Fig. 7, it could be seen that the OD600 value decreased rapidly and then approached to stabilization when penicillin, lysozyme, bovine bile salt and NaCl were added at the concentrations of 0.312 ug/mL, 0.624 mg/mL, 0.032% and 1%, respectively. This further indicates that the MIC values of penicillin, lysozyme, bovine bile salt and NaCl on *MSJA* growth were 0.312 ug/mL, 0.624 mg/mL, 0.032% and 1%, respectively.

NaCl can enter the cytoplasm through the cell membrane, which has lost its selective permeability, and inactivate *MSJA* due to the imbalance of osmotic pressure between the inside and outside of *MSJA*. Meanwhile, taurocholate can cross the collapsed cell membrane into the cytoplasm and cause DNA damage and *MSJA* inactivation. Therefore, the sensitivity of *MSJA* to NaCl and bile salts is related to the selectivity and integrity of *MSJA* cell membrane, respectively.

The sensitivity of *MSJA* organisms to the four additives can be measured by calculating the loss ratios after the addition of the four additives to the culture, using the blank group as a control, where the loss ratios are calculated as shown in Eq. 5 below.

$$D_s = \frac{Q_{vCK} - Q_{vT}}{Q_{vCK}} \quad (5)$$

where:

D_S - loss ratio; Q_{vCK} - survival rate of the control group, %; Q_{vT} - survival rate of treatment group, %. The calculations lead to the following: the loss ratio of *MSJA* at different moisture contents and temperatures are shown in Tables 2 and 3.

Table 2

Loss ratios of MSJA with different moisture content cultured on four additive media

Moisture content	Penicillin	Lysozyme	Bovine bile salt	NaCl
0.65	0.03±0.003 c	0.02±0.003 c	0.04±0.010 c	0.03±0.005 c
0.37	0.05±0.003 c	0.03±0.013 c	0.03±0.007 c	0.04±0.007 c
0.31	0.46±0.015 a	0.34±0.031 b	0.04±0.005 c	0.04±0.03 b
0.24	0.44±0.031 a	0.38±0.027 b	0.07±0.013 c	0.35±0.022 b
0.21	0.49±0.018 a	0.41±0.029 b	0.06±0.004 c	0.64±0.028 b
0.14	0.54±0.021 a	0.44±0.033 b	0.05±0.007 c	0.73±0.025 b
0.09	0.30±0.025 b	0.65±0.027 a	0.06±0.007 c	0.79±0.041 b
0.07	0.23±0.021 b	0.78±0.042 a	0.56±0.034 b	0.94±0.078 a
0.04	0.20±0.018 b	0.81±0.031 a	0.91±0.038 a	0.60±0.058 b

Note: The letters a, b and c in the table characterize the significant differences between the loss rates of MSJA pellets incubated with the same additive at different moisture contents.

As shown in Table 2, *MSJA* organisms were not susceptible to either penicillin or lysozyme until the moisture content was greater than 0.37, were sensitive to penicillin but not to lysozyme between moisture contents of 0.31-0.14, and were sensitive to lysozyme but not to penicillin between moisture contents of 0.09-0.04. Penicillin, as an inhibitor of peptidoglycan synthesis, inhibits synthetic repair of the cell wall and is associated with the presence or absence of reversible cell wall damage. Lysozyme can dissolve the cell wall structure of *MSJA* by hydrolysing the β-1,4-glycosidic bond of the *MSJA* broken cell wall, which is related to whether there is irreversible damage or even collapse of the cell wall. So, it can be concluded that the cell wall of *MSJA* showed reversible damage between moisture content of 0.37-0.31 and irreversible damage or even collapse between moisture content of 0.14-0.09.

MSJA was extremely insensitive to both NaCl and taurocholate when the moisture content was 0.65-0.31, more sensitive to NaCl and insensitive to taurocholate when the moisture content was 0.24-0.09, extremely sensitive to both NaCl and taurocholate when the moisture content was 0.07, insensitive to NaCl and extremely insensitive to taurocholate when the moisture content was 0.04. The inactivation of *MSJA* was caused by the fact that NaCl could enter the cytoplasm through the cell membrane which lost its selectivity. NaCl can enter the cytoplasm through the cell membrane which has lost its selectivity, so that the osmotic pressure inside and outside the bacterium is imbalanced and *MSJA* is inactivated; at the same time, taurocholate can enter the cytoplasm through the cell membrane which has collapsed, and cause damage to the DNA which is inactivated by *MSJA*; therefore, the sensitivities of *MSJA* to NaCl and taurocholate are respectively related to the selectivity and the integrity of the cell membrane of *MSJA*. Therefore, it can be concluded that the selective permeability of the *MSJA* cell membrane began to be impaired when the moisture content was between 0.31-0.24, and collapsed when the moisture content was between 0.09-0.07, and the cell membrane collapsed in a wide range when the moisture content reached 0.04.

Table 3

Loss ratio of MSJA cultured on four additive media at different temperatures

Temperature℃	Penicillin	Lysozyme	Bovine bile salt	NaCl
71	0.20±0.018 b	0.81±0.031 a	0.91±0.038 a	0.60±0.058 b
64.5	0.23±0.021 b	0.78±0.042 a	0.56±0.034 b	0.94±0.078 a
52	0.30±0.025 b	0.65±0.027 b	0.06±0.007 b	0.79±0.041 a
39.2	0.94±0.021 a	0.03±0.003 c	0.02±0.007 c	0.04±0.011 c

Note: The letters a, b and c in the table characterize the significant differences between the loss rates of MSJA pellets incubated with the same additive at different temperatures.

As shown in Table 3, *MSJA* organisms were extremely sensitive to penicillin and insensitive to lysozyme at 39.2℃, insensitive to both penicillin and lysozyme at 52℃, and insensitive to penicillin but extremely sensitive to lysozyme at 64.5℃ and 71℃. It can be deduced that the cell wall of *MSJA* bacteriophage began to suffer reversible damage near 39.2℃, and irreversible damage, such as collapse, began to 64.5℃.

MSJA organisms were extremely insensitive to both NaCl and bovine bile salts at 39.2℃, insensitive to penicillin and lysozyme at 52℃ and 64.5℃, extremely sensitive to NaCl but more sensitive to bovine bile salts at 64.5℃ and 71℃, and more sensitive to NaCl but extremely sensitive to bovine bile salts at 71℃. From this, it can be inferred that the cell membrane of *MSJA* bacteriophage began to be impaired in selective permeability near 52℃, and irreversible damage such as collapse began to occur near 71℃.

In summary, it can be concluded that the damage process of MSJA organisms during spray drying is as follows: first, reversible damage begins to occur at a water content of between 0.31-0.24 or at a temperature of 39.2°C. Subsequently, the selective permeability of the cell membrane began to be impaired at a water content of between 0.31-0.24 or a temperature of 52°C. Then, irreversible damage or even partial collapse of the cell wall began to occur at a water content of between 0.14-0.09 or a temperature of 64.5°C. Finally, irreversible damage, such as cell membrane collapse, began to occur at water contents between 0.09-0.07 or at a temperature of 71°C.

Observation of the morphology of the bacterium and cell wall damage mechanism

Using SEM at a magnification of 20,000 times, observations were made on rehydrated samples in rehydrated sample sampling cups at a sampling height of 45 cm under the four processes to investigate the effect of the size and morphology of the *MSJA* organisms on their survival rate. Dried particles with moisture content of 0.81, 0.34, 0.21, 0.09, 0.07 and 0.04 were observed in dried sample sampling cups to investigate the process of *MSJA* cell wall damage as shown in Fig. 8 and Fig. 9, respectively.

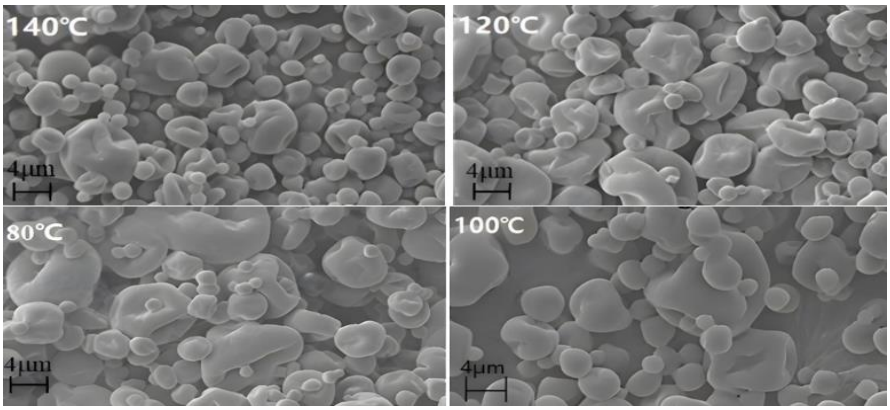

Fig. 8 - SEM scans of samples at 45 cm at each inlet temperature

As shown in Fig. 8, on the one hand, from the point of view of the average size of the bacterium, after the end of the descending-rate drying stage of spray drying, the size of the *MSJA* bacterium at different inlet temperatures was ranked as 80°C>100°C>120°C>140°C. The reason for this situation may be that the higher the hot air temperature is, the faster the water loss rate is. This may be due to the fact that, under the condition of certain material flow rate and hot air velocity, the higher the hot air temperature, the faster the water loss rate in the descending drying stage, and if the water loss rate is too fast, the more serious the dehydration damage is, which ultimately leads to the rapid contraction or even collapse of the cell wall of some bacteria. Therefore, from the point of view of the size of the bacterium (cell wall damage), the maximum inlet air temperature of spray drying should be limited to reduce the dehydration damage in the drying process of *MSJA*.

On the other hand, from the point of view of morphology and size uniformity, it is not difficult to find that with the increase of inlet temperature, the morphology of the bacterium is more similar while the size is more uniform. It may be due to the low inlet temperature, resulting in the uneven heating of the bacterial particles during atomization and descent, which ultimately led to the inconsistency of the morphology and size of the bacteria within the particles. Therefore, from the morphology and size uniformity of the bacteria, the minimum inlet temperature of spray drying should be limited. In summary, the inlet air temperature should be 100-120℃.

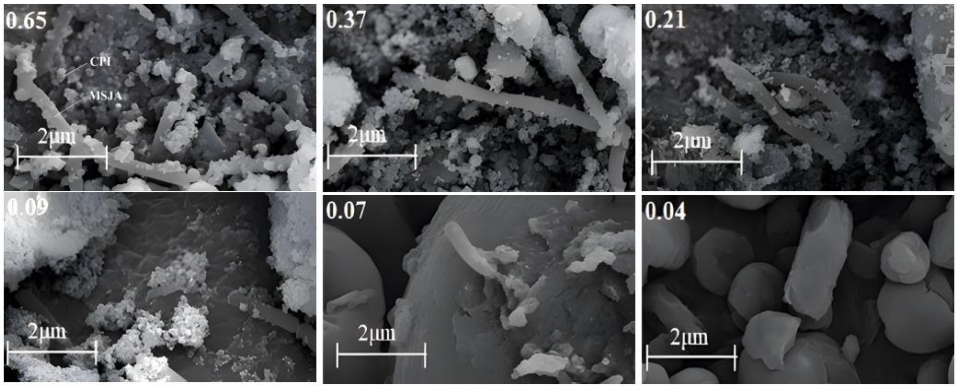

Fig. 9 - SEM scanning images of dried particles with different moisture content during the spray drying process

Observing Fig. 9, it is easy to see that the cell walls of the majority of *MSJA* organisms can remain intact and smooth before the moisture content is higher than 0.21, but as the moisture content drops to 0.07, the cell walls of the *MSJA* organisms gradually begin to shrink or even rupture. Because the rapid inactivation of *MSJA* occurs between 0.21-0.34 moisture content, it can be concluded that the cell wall is one of the sites of inactivation of *MSJA* organisms, but it is not the key site.

Analysis of damage to cell membrane fatty acids, proteins and DNA

The FTIR second-order derivative profiles at three bands are shown in Fig. 10 (a) - (c), respectively.

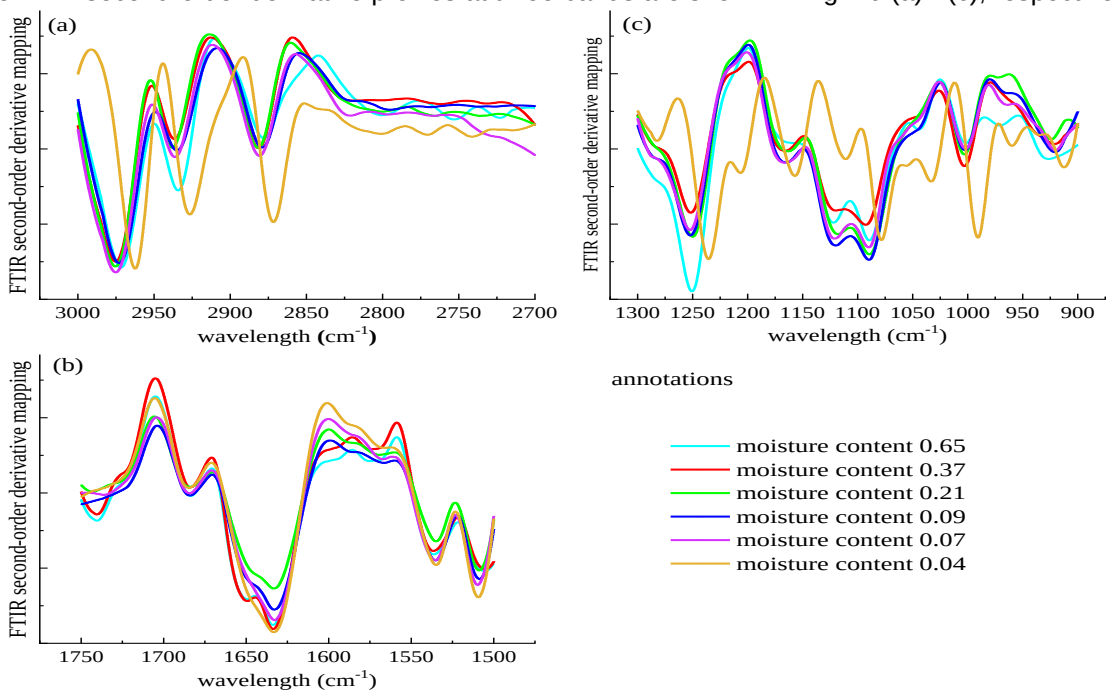

Fig. 10 - FTIR second-order derivative mapping

As shown in Fig. 10 (a), the FTIR second-order derivative patterns of *MSJA* particles with different moisture contents all showed obvious absorption peaks in the regions near the wavelengths of 2950 cm^{-1}, 2900 cm^{-1} and 2850 cm^{-1}, which were closely related to the composition and phase transition of the cell membrane lipids of the *MSJA* organisms. The absorption peaks near 2950 cm^{-1} and 2900 cm^{-1} were related to the symmetric expansion and contraction of CH_3 and CH_2 in the lipid acyl groups of the cell membrane, i.e., the gel phase transition of the cell membrane, and the absorption peaks near 2850 cm^{-1} were related to the asymmetric expansion and contraction of CH_3 and CH_2 in the lipid acyl groups of the cell membrane, i.e., the anti-hexagonal phase transition of the cell membrane. At the wavelengths of 2950 cm^{-1} and 2900 cm^{-1}, the absorption peaks gradually shifted to 2935 cm^{-1} and 2875 cm^{-1} when the moisture content was lower than 0.21, and the peak heights were also gradually increased. This indicates that the van der Waals force between the bilayer phospholipid molecules of the *MSJA* cell membrane increases at moisture content of 0.21, and the gel phase transition occurs, and the selective permeability of the cell membrane is also damaged.

At the wavelength of 2850 cm^{-1}, the peak height of the absorption peak was dramatically lowered when the moisture content was lower than 0.07. This indicates that at moisture content of 0.04, the cell membrane of *MSJA* bacteriophage begins to undergo an anti-hexagonal phase transition and thus begins to collapse. This is consistent with the two critical moisture content points for the massive death of *MSJA*, indicating that the gel phase transition and the anti-hexagonal phase transition of the cell membrane at moisture content of 0.21 and 0.07, respectively, are the key causes of the death of *MSJA* during the spray-drying process.

As shown in Fig. 10 (b), the FTIR second-order derivative patterns of *MSJA* particles with moisture contents of 0.065 and 0.037 both showed fluctuation peaks at wavelengths ranging from 1660 cm^{-1} to 1635 cm^{-1} associated with protein β-turns and α-helices, respectively. And the fluctuation peaks were obviously weakened as the moisture content decreased to 0.21 and 0.09, and the fluctuation peaks completely disappeared as the moisture content decreased to 0.07. The α-helix and β-rotor are an ordered structural component of proteins, and the disappearance of the α-helix and β-rotor implies that the protein structure in the bacterium has been irreversibly damaged. It means that the proteins in the bacterium begin to suffer reversible damage when the moisture content is 0.21, and the proteins in the bacterium begin to suffer irreversible damage when the moisture content is 0.07.

As shown in Fig. 10 (c), the FTIR second-order derivative patterns of *MSJA* particles at each moisture content all showed distinct absorption peaks closely related to the symmetric and asymmetric scaling of PO^{2-} in the DNA ribosome in the region near the wavelengths of 1200 cm^{-1} and 1040 cm^{-1}, respectively. The symmetric expansion of PO^{2-} in DNA started to move slowly to the right to 1195 cm^{-1} when the moisture content reached 0.07, and finally moved rapidly to 1180 cm^{-1} when the moisture content was 0.04. The asymmetric expansion of PO^{2-} in DNA suddenly moved rapidly to 1010 cm^{-1} when the moisture content reached 0.04. The symmetric expansion of PO^{2-} in DNA was also found in the region near 1200 cm^{-1} and 1040 cm^{-1}. It indicates that the DNA of *MSJA* bacteriophage started to suffer reversible and non-lethal damage at moisture content of 0.07, and started to suffer greater damage only at moisture content lower than 0.04.

CONCLUSIONS

During the spray-drying process of *MSJA*, although the cell wall was damaged first, this damage did not directly lead to the death of MSJA; it was the immediately following cell membrane damage that was the most critical to directly cause the death of *MSAJ*. The critical temperature and moisture content for the cell membrane phospholipid bilayer to undergo gel phase transition, leading to the death of MSJA, were 52℃ and 0.21℃, respectively, while the critical temperature and moisture content for the cell membrane phospholipid bilayer to undergo anti-hexagonal phase transition or even disintegration, leading to the death of a large number of MSJA, were 71℃ and 0.07℃, respectively.

When the drying water content was lower than 0.21, the phase transition of the phospholipid bilayer resulted in the loss of selective permeability of the cell membrane, which was the key factor leading to the death of MSJA. Only when the water content was lower than 0.04, protein damage in the bacterium caused MSJA death, and the effect of DNA damage on MSJA death was almost negligible.

The hot air inlet temperature and outlet temperature of spray drying should be limited to 100-120℃ and 48-52℃ respectively.

ACKNOWLEDGEMENT

This work was supported by the National Natural Science Foundation of China [grant number 51876109]; the key R&D Program Project of Shaanxi Provincial [grant number 2021NY-129]; and the Scientific research plan project of youth innovation team of Shaanxi Provincial Department of Education [grant number 22JP012].

REFERENCES

[1] Al Zaitone, B.; Al-Zahrani, A.; Ahmed, O.; Saeed, U.; Taimoor, A.A. (2022). Spray Drying of PEG6000 Suspension: Reaction Engineering Approach (REA) Modeling of Single Droplet Drying Kinetics. *Processes*. 10, 1365. https://doi.org/10.3390/pr10071365.

[2] Cheng, S.S.; Su, W.T.; Yuan, L.; Tan, M.Q. (2021). Recent developments of drying techniques for aquatic products: With emphasis on drying process monitoring with innovative methods. *Drying Technology*. 39(11), 1577-1594. https://doi.org/10.1080/07373937.2021.1895205.

[3] Cheng, W.; Chen, X.F.; Zhou, D.; Xiong, F.K. (2022). Applications and prospects of the automation of compound flavor baijiu production by solid-state fermentation. *International journal of food engineering*. 12(18), 737–749. https://doi.org/10.1515/ijfe-2022-0200.

[4] Dukic, N.; Radonjic, A.; Popovic, B.; Andric, G. (2021). Development and progeny performance of Tribolium castaneum (Herbst) in brewer's yeast and wheat (patent) flour at different population densities. Journal of Stored Products Research. 94, 101886. https://doi.org/10.1016/j.jspr.2021.101886.

[5] Fang, L.; Yang, W.; Hou, J.H; Zheng, K.W.; Hussain, A.; Zhang, Y.C.; Hou, Z.H.; Wang, X.Z. (2023). Tofukasu-derived biochar with interconnected and hierarchical pores for high efficient removal of Cr (VI). *Biochar*. 5(1), 69. https://doi.org/10.1007/s42773-023-00268-0.

[6] Gong, P.M.; Sun, J.L.; Lin, K.; Di, W.; Zhang, L.W.; Han, X. (2018). Changes process in the cellular structures and constituents of Lactoba-cillus bulgaricus sp1.1 during spray drying. *LWT- Food Sci. Technol*. 102, 30–36. https://doi.org/10.1016/j.lwt.2018.12.005.

[7] Gómez-Narváez, F.; Díaz-Osorio, A.; Gómez-Narváez, S.; Simpson, R.; Contreras-Calderón, J. (2023). Modeling the impact of spray drying conditions on some Maillard reaction indicators in nano-filtered whey. *Journal of food process engineering*. 46(1), 14212. https://doi.org/10.1111/jfpe.14212.

[8] Kandasamy, S.; Naveen, R. (2022). A review on the encapsulation of bioactive components using spray-drying and freeze-drying techniques. Journal of food process engineering. 45(8), 14059. https://doi.org/10.1111/jfpe.14059.

[9] Izu, H.; Yamashita, S.; Arima, H.; Fujii, T. (2018). Nutritional characterization of sake cake (sake-kasu) after heat-drying and freeze-drying. *Bioscience Biotechnology & Biochemistry*. 83(8), 1-7. https://doi.org/10.1080/09168451.2018.1559723.

[10] Liu, Z.; Xu, L.; Wang, J.; Duan, C. (2023). Research progress of protein haze in baijius. Food Science and Human Wellness. 12(5), 1427-1438. https://doi.org/10.1016/j.fshw.2023.02.004.

[11] Noghabi, M.S.; Molaveisi, M. (2020). Microencapsulation optimization of cinnamon essential oil in the matrices of gum Arabic, maltodextrin, and inulin by spray-drying using mixture design. *Journal of Food Process Engineering*. 43, 13341. https://doi.org/10.1111/jfpe.13341.

[12] Paup, V.D.; Barton, T.L.; Edwards, C.G.; Lange, I.; Lange, B.M.; Lee, J.; Ross, C.F. (2016). Influence of polysaccharides on the taste and mouthfeel of white wine. *Australian Journal of Grape and Wine Research*. 22(3):350-357. https://doi.org/10.1111/1750-3841.16371.

[13] Samborska, K.; Edris, A.; Jedlinska, A.; Baranska, A. (2021). The production of white mulberry molasses powders with prebiotic carrier by dehumidified air-assisted spray drying. *Journal of Food Process Engineering*. 45, 13928. https://doi.org/10.1111/jfpe.13928.

[14] Spreutels, L.; Haut, B.; Chaouki, J.; Bertrand, F. (2014). Conical spouted bed drying of Baker's yeast: Experimentation and multi-modeling. *Food Res. Int.* 62, 137–150. https://doi.org/10.1016/j.foodres.2014.02.02.

[15] Wang, Y.; Huang, X.Y.; Aheto J.; Ren, Y.; Zhang, X.; Wang, L. (2021). Novel colorimetric sensor array for Chinese rice wine evaluation based on color reactions of flavor compounds. *Journal of food process engineering*. 44(12), e13889. https://doi.org/10.1111/jfpe.13889.

[16] Xiong, F.K.; Yuan, Y.J.; Xu, Y.Y.; Li, J.Y.; Zhao, Z.; Tan, L.B. (2022). Modeling Study of a Microbial Spray-Drying Process Based on Real-Time Sampling. *Processes*. 10, 1789. https://doi.org/10.3390/pr10091789.

[17] Yang, H.; Huang, P.; Hao, L.Y.; Che, Y.L.; Dong, S.R.; Wang, Z.H.; Wu, C.D. (2023). Enhancing viability of dried lactic acid bacteria prepared by freeze drying and spray drying via heat preadaptation. *Food Microbiology*, 112,104239. https://doi.org/10.1016/j.fm.2023.104239.

[18] Yuan, Y.J.; Xiong, F.K.; Li, J.Y.; Xu, Y.Y.; Zhao X.T. (2022). Review on Drying Technology and Damage Protection Mechanism of Liquor Yeast. *INMATEH - Agricultural Engineering*. 68 (3) 735-746. https://doi.org/10.35633/inmateh-68-73.